Applied Catalysis B: Environmental 313 (2022) 121439

Contents lists available at ScienceDirect

Applied Catalysis B: Environmental

journal homepage: www.elsevier.com/locate/apcatb

Ambient photothermal catalytic CO oxidation over a carbon-supported palladium catalyst

Ziwen Liu, Lijuan Niu, Xupeng Zong, Li An, Dan Qu, Xiayan Wang, Zaicheng Sun *

Center of Excellence for Environmental Safety and Biological Effects, Beijing Key Laboratory for Green Catalysis and Separation, Department of Chemistry and Biology, Faculty of Environment and Life, Beijing University of Technology, Beijing 100124, China

ARTICLE INFO

Keywords:
Photothermal
Catalytic CO oxidation
Carbon
Palladium
Local temperature

ABSTRACT

The XC-72R supported Pd catalysts exhibit low-temperature catalytic activity for CO oxidation under light irradiation. The CO conversion can reach 100% with the light irradiation of 900 mW·cm^{-2} at a catalyst temperature of 100 °C. Pd/C catalysts with different Pd loading have similar performance enhancement under light irradiation. The activation energy of 1% Pd/C catalyst remains unchanged implying that CO oxidation belongs to photothermal catalytic oxidation. The enhanced performance could be ascribed to ultrahigh surface temperature (275 °C) induced by the light irradiation of 800 mW·cm^{-2} and detected by an IR camera. That is higher than the catalyst temperature (187 °C) measured by the thermocouple. Carbon generates a higher temperature than Pd NP, causing heat transfers from carbon to Pd NP. In contrast, Pd NP produces a higher temperature than Al_2O_3 for Pd/Al_2O_3 catalyst, and heat is transferred from Pd to Al_2O_3. These demonstrate that the enhanced performance contributes to the photothermal effect of carbon.

1. Introduction

CO oxidation is one of the most widely studied reactions in the field of heterogeneous catalysis due to its significance in environmental protection and fundamental studies [1]. Noble metals (Au, Pt, Pd, and others) have been demonstrated as highly active catalysts for CO oxidation [2–5]. And a considerable strategy has been devoted to developing low-temperature CO oxidation catalysts to lower the reaction temperature by constructing metal/oxides [6–8]. However, a higher reaction temperature is still needed generally provided by the traditional electrical heater to activate the oxidation, which results in energy consumption and environmental pollution [9,10]. Sunlight consists of 5% of ultraviolet (UV), 46% visible and 49% infrared (IR) light, respectively [11]. Consequently, it is considered an alternative and highly efficient heat source since light energy can be converted into heat by photothermal materials. Another merit is that the specific site can be heated up without heating the surrounding environment with photothermal materials. For example, the surface water is heated by photothermal material in interfacial water evaporation [12,13]. This strategy can be applied to CO oxidation by making use of the photothermal properties of the catalyst [14,15]. The light can be effectively converted to heat and raise the temperature of the catalyst, which could enhance the catalytic performance of the catalyst [16,17]. Therefore, it is great potential to make use of the photothermal materials to boost the catalytic performance of CO oxidation at the catalyst site within a short period.

Carbon is common catalyst support due to its properties of the highly tunable structure, chemical inert, low cost, and earth-abundance [18]. Besides, it also is an excellent photothermal material owing to full-spectrum absorption. Liu and coworkers designed hierarchical graphene foam as the solar absorber, which has high solar spectrum absorption in the range of 295–2500 nm with the lowest transmittance (≈ 0%) and exceptional photo-thermal conversion efficiency up to 93.4%. The temperature could reach 145 °C under the irradiation intensity of 5 kW·m^{-2} [19]. A similar phenomenon was also reported by other groups [20,21]. Pd/porous carbons show relatively low full conversion temperature and good catalytic activity for CO oxidation [22–24]. However, it is still far behind than noble metal/oxides catalyst due to weak interaction between noble metal and carbon support [25]. However, carbon is a good candidate for understanding the photothermal catalytic oxidation of CO if considered as catalyst support and photothermal materials with full-spectrum light absorption. Meanwhile, the carbon-based supported noble catalysts are used for thermal catalytic CO oxidation, but their application in photothermal catalytic CO

* Corresponding author.
E-mail address: sunzc@bjut.edu.cn (Z. Sun).

https://doi.org/10.1016/j.apcatb.2022.121439
Received 29 March 2022; Received in revised form 18 April 2022; Accepted 21 April 2022
Available online 25 April 2022

oxidation has rarely been investigated so far.

In this work, we choose a commercial carbon (XC-72R) as catalytic support and employ a simple PVA-protected reduction strategy to prepare Pd/C catalysts for the photothermal catalytic oxidation of CO. The synthesized Pd/C catalysts exhibited remarkably catalytic performance under light irradiation, which was much better than in dark conditions. The 100% CO conversion temperature (TF_{100}, furnace temperature) of 1% Pd/C catalyst from 146 °C dropped down to 30 °C under light irradiation with the intensity of 900 mW·cm^{-2}. The superior performance of Pd/C catalysts was attributed to the ultra-high local temperature detected by the IR camera which was produced by carbon support due to its excellent photothermal conversion ability than Pd species. And IR light is the main contributor to performance enhancement analyzed by introducing the cut-off optical filter. We believe that this work could provide a more fundamental understanding of other photothermal catalytic oxidation reactions and more possibilities for utilizing solar energy fully with the employ of carbon materials.

2. Experimental

2.1. Material and methods

2.1.1. Materials

All chemicals were used as received without further purification. Polyvinyl alcohol (PVA, 98–99% hydrolyzed, low molecular weight) and Aluminum oxide (Al_2O_3, NanoTek, 99.5%) were purchased from Alfa Aesar (China) Chemicals Co., Ltd. Na_2PdCl_4 (99.9%) and $NaBH_4$ (AR 98.0%) were obtained from J&K Chemical. Cabot Vulcan XC-72R was purchased from Shanghai Macklin Biochemical Co., Ltd. Activated carbon was purchased from TCI (Shanghai) Development Co., Ltd.

2.1.2. Catalyst preparation

The synthesis of Pd/C catalysts through a PVA-protected reduction strategy. The detailed process is as shown below: The desired amount of PVA (noble metal/PVA mass ratio = 1:1.5) was added to a Na_2PdCl_4 aqueous solution in an ice bath under vigorous stirring for 20 min. After rapidly injecting the $NaBH_4$ (2 g/L, noble metal/$NaBH_4$ molar ratio = 1:5), a dark sol was generated. Then a certain weight XC-72R was added to the above dark sol under stirring until complete adsorption was achieved. The obtained mixture was filtered, washed with deionized water, dried at 80 °C overnight. Then as-produced sample was calcined in air at a heating rate of 5 °C/min from RT to 180 °C and maintained this temperature for 3 h. The obtained sample was the Pd/C catalyst. The loading of Pd species was adjusted by controlling the addition amount of XC-72R. Pd/Al_2O_3 catalyst was prepared by similar methods just to replace XC-72R with Al_2O_3. The actual loading of catalysts was determined by ICP-AES shown in Table S1.

2.2. Catalytic performance of CO oxidation

CO oxidation catalytic activities were evaluated in a continuous flow, fixed-bed quartz reactor (i.d. = 8 mm) with a flat quartz window to allow light irradiation. 50 mg catalyst mixture with 450 mg quartz sand was fixed in the flat quartz window of the reactor by packing quartz wool at both ends. A thermocouple was placed in direct contact with the catalyst for the catalyst temperature (TC) measurements. The total flow rate of the reaction gas mixture was 50 mL/min, which contained 1% CO, 20% O_2, and Ar as balance gas. The corresponding space velocity (SV) was 60,000 mL·(g·h)$^{-1}$. The concentration of CO in the inlet and outlet of the reactor was analyzed by gas chromatography (Shimadzu GC-2014 C) using a thermal conductivity detector (TCD), with argon as the carrier gas. A xenon lamp (Microsolar 300 from Beijing Perfectlight) was used to provide a certain intensity of light radiation. The cross-section of the reactor is drawn in Fig. S1.

The detailed catalyst characterizations and catalytic evaluation procedures are described in the Supporting Information (SI).

3. Result and discussion

3.1. Characterization of catalysts

Fig. 1a presents the X-ray diffraction (XRD) patterns of Carbon support and Pd/C with different loading amounts. The Vulcan XC-72R exhibits its typical diffraction peaks at 2θ = 24.8° and 43.4°. It is hard to observe Pd diffraction peaks for the 1.0% Pd/C. The intensity of Pd diffraction peaks increases with the Pd loading amount on the carbon support. The diffraction peaks at 39.9º, 46.4º, 68.0°, and 82.0° are observed in the XRD pattern of Pd/C, which can be attributed to the (111), (200), (220), and (311) planes of Pd nanoparticles (JCPDS no. 46–1043). The morphology and particles size of Pd/C was characterized by transmission electron microscopy (TEM, Figs. 1b–c and S2). The Pd nanoparticles were uniformly dispersed on the carbon spheres. The average particle sizes of Pd nanoparticles are 3.66 ± 0.67 nm, 3.92 ± 0.72 nm, 4.05 ± 0.81 nm and 4.22 ± 0.93 nm corresponding to 1.0%, 2.0%, 4.0% and 6.0% weight amount in the Pd/C catalysts, respectively. A high-resolution TEM image (Fig. 1c) discloses the Pd nanoparticles with a lattice fringe spacing of 0.22 nm is corresponding to the (111) plane of Pd. The valence state of Pd/C was evaluated by X-ray photoelectron spectroscopy (XPS). As shown in Fig. 1d, the XPS spectra of Pd $3d_{5/2}$ can be fitted with three peaks, which could be assigned to Pd^0 [26], Pd^{2+} [27], and Pd^{4+} species [28], indicating three different kinds of chemical states co-exist in this sample. In Fig. 1e, C1s XPS spectra are depicted which can be de-convoluted into five peaks, assigned to C═C-C (sp^2 C), C-OH, C-O-C, HO-C═O, and π-π * bonds, respectively. And in Fig. 1f, O 1s XPS spectra could decompose into two peaks, ascribed to C-O and O-C═O species in XC-72R [29,30]. From the nitrogen adsorption-desorption isotherms, the XC-72R displayed a hybrid of type I and Ⅳ nitrogen adsorption-desorption isotherm (Fig. S3), which slightly steep uptake of N_2 at very low relative pressure ($P/P_0 < 0.01$) indicating the presence of micropore, an H3 hysteresis loop at relatively high pressure suggesting the presence of mesopores. And the surface area, pore-volume, and average pore size were 284.6 m^2/g, 0.65 cm^3/g, and 9.1 nm respectively (Table S2).

3.2. Light-driven photothermal catalytic performance

The optical properties of the material are one of the significant factors that impact the photothermal catalytic activity [17]. Therefore, the UV-Vis-IR diffuse reflection spectroscopy (DRS) was carried out to investigate the light absorption capacity. All catalysts exhibit a similar strong absorption in the range of 200–2500 nm with a rather lower reflectance (< 11% in the visible region, ≈ 6.5% in the near-infrared region, and < 6% in the infrared region) (Fig. 2a). The light absorption capability has no obvious enhancement even after loading Pd nanoparticles, indicating that Pd nanoparticle has a negligible contribution to light absorption.

The catalytic activities of all samples for CO oxidation are both evaluated under dark conditions and light irradiation with the intensity of 500 mW·cm^{-2}. In the dark condition, the pure carbon support has no catalytic activity even the temperature was elevated to 180 °C. The catalytic performance of catalysts is gradually improved by loading Pd nanoparticles. The lowest total conversion catalyst temperature (TC_{100}) is 167 °C, 160 °C, 148 °C and 142 °C, corresponding to 1.0%, 2.0%, 4.0% and 6.0% weight amount in the Pd/C catalysts, respectively (Fig. 2b). Upon irradiation, the catalyst temperature of all samples is rapidly risen to 66 °C within 5 min, then reach 75 °C for 10 min. Finally, it maintains at the 78 °C for 15 min (Fig. 2c). The sample temperature is independent on the Pd loading, indicating that the application of photothermal effect is an effective and rapid method to heat up the catalyst. However, it exhibits no catalytic activity for pure carbon even under light irradiation (Fig. 2b). The overall catalytic performance of Pd/C is enhanced when light is irradiated on the samples, indicating that the Pd species are active sites for CO oxidation. TC_{100} decreases to 119 °C,

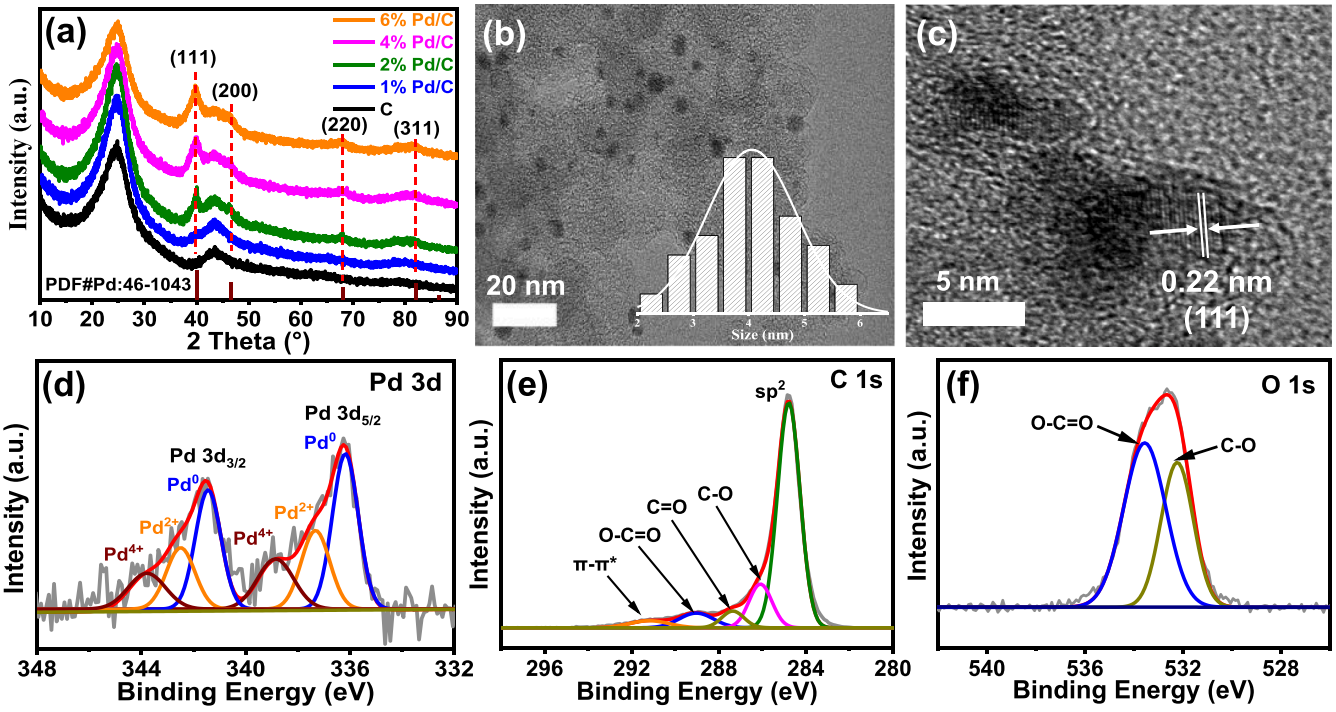

Fig. 1. (a) XRD patterns of Pd/C catalysts, (b) TEM and (c) HRTEM of 1% Pd/C catalyst, insert of (b):particle size distribution, and (d-f) XPS patterns of 1% Pd/C.

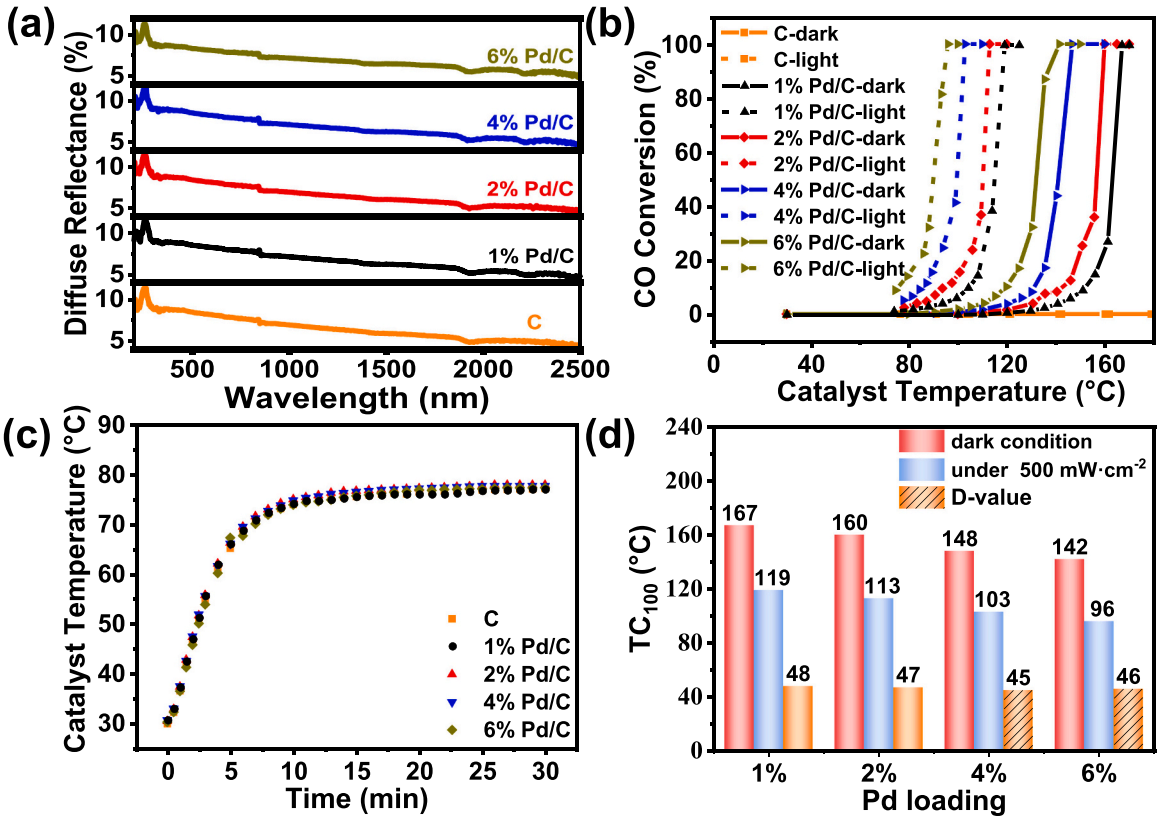

Fig. 2. (a) UV–vis–IR DRS spectra of Pd/C and C, (b) CO conversion of C support and Pd/C catalysts under dark conditions and the light irradiation of 500 mW·cm^{-2}, (c) catalyst temperature of samples under 500 mW·cm^{-2}, (d) The TC_{100} and D-value between dark and light irradiation of 500 mW·cm^{-2} over Pd/C catalysts.

113 °C, 103 °C, and 96 °C for different Pd loading catalysts, respectively. Compared to the enhanced degree of catalysts, the D-value (the difference in TC_{100} between dark and lighted conditions) are 48 °C, 47 °C, 45 °C, and 46 °C, respectively (Fig. 2d). All catalysts have a similar enhancement, indicating Pd loading seems not to be the major contributor to photo-assisted catalytic activity enhancement.

Furthermore, the influence of light intensity on photothermal catalytic activities is investigated for a 1% Pd/C sample. The catalyst temperature of 1% Pd/C gradually elevates to an equilibrium temperature of 52 °C, 67 °C, 83 °C, 94 °C, and 105 °C within 15 min under 200, 400, 600, 750, and 900 mW·cm^{-2} light irradiation, respectively. The equilibrium temperature of catalysts increased linearly with the increase of illumination intensity, as depicted in Fig. S4. The heating rate of catalyst temperature is significantly accelerated with the increased light intensity, and its maximum heating rate can reach 4.4 °C/min, 9.6 °C/min, 12.2 °C/min, 15.5 °C/min, and 19.1 °C/min corresponding to 200, 400, 600, 750 and 900 mW·cm^{-2} light intensity, respectively (Fig. 3a).

Fig. 3b shows the curve of CO conversion with a catalyst temperature of samples under dark and different illumination intensity conditions. In the dark condition, the TC_{100} is 167 °C for 1% Pd/C samples. When the light intensity increases from 200 to 900 mW·cm^{-2}, the TC_{100} is gradually decreased from 140 °C to 100 °C, indicating the catalytic activity of the Pd/C catalyst is greatly improved and strongly related to the light intensity. Since two heat sources are contributing to the catalyst temperature in CO oxidation. One is an external heat source (furnace), another is from photothermal material (carbon support and/or Pd), which converts the light to heat. To better distinguish the contribution of these two, the plot of CO conversion with furnace temperature (TF) detected by thermocouple II (Fig. S1) was redrawn as Fig. 3c. It requires the TF of 146 °C to achieve complete conversion of carbon monoxide under dark conditions. Nonetheless, it only needs an ambient temperature (TF=30 °C) to reach 100% conversion under the irradiation intensity of 900 mW·cm^{-2}. At the moment, the CO could be ultra-fast completely converted within 10 min once irradiation arrived at 900 mW·cm^{-2} (Fig. S5). Based on the above, it can be concluded that light intensity plays a pivotal role in the catalytic reaction.

To investigate the intrinsic activity of Pd/C, the turnover frequency of Pd (TOF_{Pd}) is calculated as shown in Fig. 3d. In dark condition, the TOF merely reach 0.97 × 10^{-3} s^{-1} under 110 °C, while the TOF increased to 21.06 × 10^{-3} s^{-1} at 100 °C the irradiation intensity of 600 mW·cm^{-2}, which is 21.7 times higher than that under the dark condition. Compared with the supported Pd catalyst reported in literature, the TOF_{Pd} value over Pd/C under light of 600 mW cm^{-2} is higher than over 10 wt% Pd/graphene (9.28 ×10^{-3} s^{-1})) [22], 1.2 wt% Pd/$SrTiO_3$ (4.1 ×10^{-3} s^{-1})) [31].

3.3. Mechanism of photothermal enhancement of catalytic performance

The catalytic activity of the Pd/C catalyst was remarkedly enhanced after irradiation of light. Therefore, it is essential to probe the mechanism of enhanced catalytic activity. Firstly, we performed a set of experiments to measure the apparent activation energy (E_a) of a 1% Pd/C catalyst. As shown in Fig. 4a, the corresponding activation energy is 112.9 kJ mol^{-1} under dark conditions, and E_a has barely changed after the introduction of light, indicating that light irradiation could not change the E_a. A similar phenomenon also happened in the photomethanation over Ru/Silicon nanowire [32]. It has been reported that Pd metal is not a plasmonic metal and the surface plasmon resonance absorption is rather weak [33]. In addition, the absorption of the smaller Pd particles (size less than 10 nm) is generally located at 200–250 nm ascribed to the UV part [34]. Due to the existence of interband electronic transitions and intraband transitions, the Pd nanoparticles have noticeable optical absorption in the visible and near-infrared wavelength range, which could be regarded as “nano heaters” to increase the local temperature of catalysts [35]. Here, considering the carbon is inert support, we could conclude that the enhanced catalytic activity mainly comes from the light-driven thermal catalysis, and no photocatalytic reaction occurs in our cases. Furthermore, we also tested the catalytic activity of the 1% Pd/C catalyst with the temperature controlled by water circulation under the light irradiation of 900 mW·cm^{-2} as shown in Fig. S6. When the catalyst temperature is set at a low temperature (30–60 °C), the catalyst displays no catalytic activity, indicating catalyst

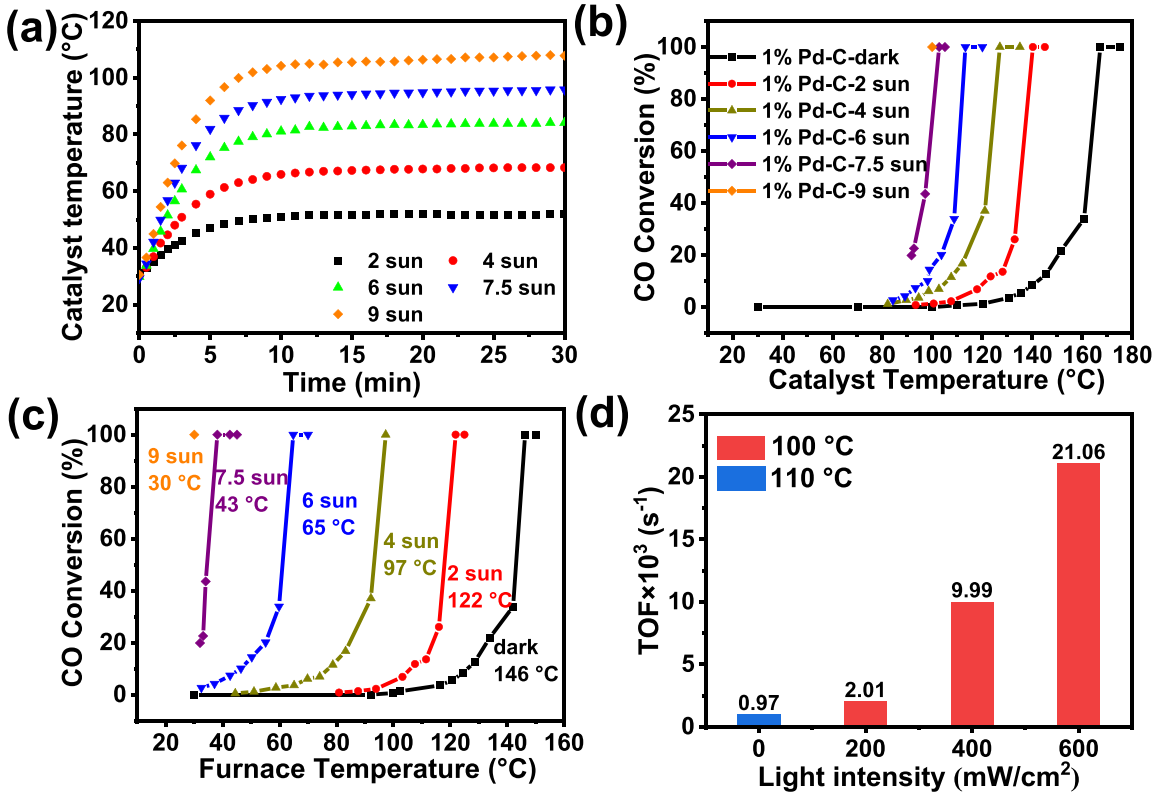

Fig. 3. (a) Catalyst temperature of 1% Pd/C under different light intensity; (b)-(c) Catalyst and furnace temperature dependence of CO conversion over 1% Pd/C samples with different light irradiation intensity; (d) TOF values at 100 °C and 110 °C for 1% Pd/C under different light intensity.

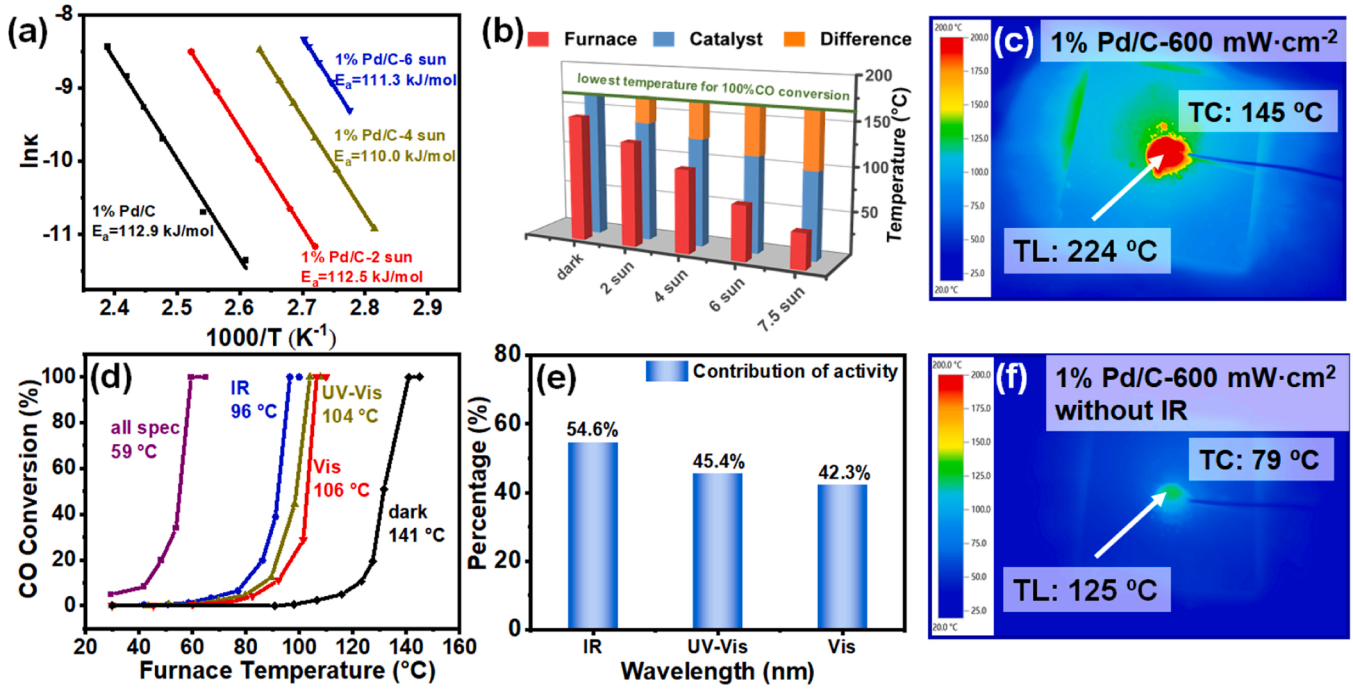

Fig. 4. (a) Arrhenius plots for CO oxidation over 1% Pd/C catalyst under different light intensity; (b) The value of TC_{100} and TF_{100} over 1% Pd/C catalysts; (c) IR image over Pd/C catalyst under light irradiation with the light intensity of 600 mW·cm^{-2}; (d) CO conversion over 1% Pd/C under different wavelengths with an initial light intensity of 600 mW·cm^{-2}; (e) Contribution ratio of activity enhancement at different wavelength ranges over 1% Pd/C catalyst; (f) IR image over Pd/C catalyst without IR light irradiation with the light intensity of 600 mW·cm^{-2}.

temperature plays a critical role in CO oxidation. When light is irradiated on the catalyst, the Pd/C catalysts could convert the absorbed light into heat, which increases the local temperature of catalysts, while the ambient temperature remains essentially unchanged. According to the dark condition of CO oxidation, CO can be fully converted when the catalyst site (TC_{100}) reaches 167 °C. TC_{100} only reaches 100 °C and it attains full conversion in the case of 900 mW·cm^{-2} light irradiation, indicating the catalyst site has been reached 167 °C although the apparent catalyst temperature is 100 °C. In other words, the actual temperature of the catalytic site is higher than the apparent catalyst temperature. Therefore, we proposed a concept of the local temperature (TL), which is the actual temperature at the catalyst surface. Since the CO can be fully converted, the TL_{100} should be equal to the TC_{100} under dark conditions. Fig. 4b presents the TF, TC, and difference between TF_{100} under light irradiation state and TC_{100} under dark state. The difference strongly depends on the light intensity, indicating that the photothermal materials generate heat at the surface site. To verify this, both the thermocouple and IR camera are employed to detect the TC and TL, respectively (Figs. 4c, S7, and S8). TC and TL are about 79 °C and 114 °C for 1% Pd/C under 200 mW·cm^{-2} light irradiation. When the light intensity increases to 400, 600, and 800 mW·cm^{-2}, TC turns 116 °C, 145 °C, and 187 °C, and TL increases to 165 °C, 224 °C, and 275 °C, respectively. Both TC and TL increase significantly with increasing light intensity. The difference between TC and TL becomes from 35 °C to 88 °C, manifesting that TL is higher than TC. That is the reason why the CO can be fully converted at a relatively low TC (103 °C) under light irradiation. That is the advantage of photothermal materials which can fulfill high temperatures at the local position of photothermal materials and low temperatures in the environment.

To disclose the contribution from the light irradiation, the catalytic activities of Pd/C under different wavelengths of light radiation were carried out. The heat comes from two sources the external electrical furnace and the photothermal effect. Fig. 4d exhibits the plot of CO conversion vs. the furnace temperature with different wavelengths of light. TF_{100} is about 141 °C under a dark state, while TF_{100} is 59 °C under full-spectrum light of 600 mW·cm^{-2}. That indicates that the temperature difference (82 °C) is made up of heat from light. To understand the wavelength effect, the cut-off optical filter is applied to tune the light wavelength range, When the 800 nm cut-off optical filter is applied, the TF_{100} turns to 96 °C. It implies that the IR light contributes to the temperature difference of 45 °C. UV–vis light (200–800 nm) contributes to the temperature difference of 37 °C. And visible light (400–800 nm) contributes to the temperature difference of 35 °C. Considering the full-spectrum light as a 100% contribution to the catalytic activity, then the IR light ($\lambda > 800$ nm) contributes about 54.6%. The UV–vis light ranging from 200 nm to 800 nm is responsible for 45.4% and the visible light (400–800 nm) promotes the catalytic activity of 42.3% (Fig. 4e). It implies that IR light is a dominant part of the whole spectrum of light for catalytic CO oxidation. When IR light was filtered, TC and TL are significantly reduced indicating the IR light play a significant role in raising the TL, which is consistent with the results of activity change (Fig. 4f).

To verify the function of photothermal material-carbon support, Al_2O_3 is chosen as a non-photothermal reference. The Al_2O_3 sample exhibited a type Ⅳ nitrogen adsorption-desorption isotherm with an H3 hysteresis loop (Fig. S9), indicating the presence of mesopores only. And the surface area, pore-volume, and average pore size were 155.8 m^2/g, 1.31 cm^3/g, and 3.36 nm respectively (Table S2). And 1% Pd/Al_2O_3 catalyst was synthesized to compare with the Pd/C sample. TEM images show the average particle size of Pd nanoparticles is 3.44 ± 0.58 nm, similar to the size of 1% Pd/C (Fig. S10a and b). While the Pd/Al_2O_3 catalyst possesses higher reflectance with a minimum value of around 21%, far than Pd/C catalysts (around 3%) shown in Fig. S11. In the following, the catalytic activity under light irradiation with different wavelengths was also investigated. As shown in Fig. S12a, the performance of the Pd/Al_2O_3 catalyst is also enhanced to some extent, and TF_{100} decreases from 129 °C in dark conditions to 72 °C under full-spectrum irradiation, similar to Pd/C samples. In addition, with the different optical filters, the catalytic activity decreases either. According to the result of contribution and spatial temperature mapping

(Fig. S12b–d), the IR irradiation with a 52.3% contribution plays a major role in catalytic activity and elevating surface temperature. And the Pd/Al_2O_3 system also follows the light-driven thermal catalysis.

Fig. 5a presents the plot of CO conversion vs. TF of Pd/C and Pd/Al_2O_3. At dark condition, Pd/Al_2O_3 sample exhibits better performance (TF_{100} = 124 °C) than Pd/C catalyst (TF_{100} = 142 °C) since C is inert. When the light (600 mW·cm^{-2}) is applied, the catalytic activity of both samples is enhanced. Pd/C displays lower TF_{100} (55 °C) than Pd/Al_2O_3 (TF_{100} = 72 °C), indicating Pd/C can generate more heat to elevate the surface temperature than Pd/Al_2O_3 under the same light intensity. To understand the enhancement mechanism, the TL of each component including Pd nanoparticles, C, Al_2O_3, Pd/C, Pd/Al_2O_3 are investigated by an IR camera under the same light intensity. Considering the stability of Pd nanoparticles, the light intensity is set to 200 mW·cm^{-2} (Fig. 5b–g). The TL is 112 °C, 131 °C, 62 °C, 120 °C, and 96 °C corresponding to Pd, C, Al_2O_3, Pd/C, and Pd/Al_2O_3 samples, respectively. Although Pd is considered non-photothermal materials, both TL and TC increase and TL is higher than TC under light irradiation, implying that Pd nanoparticles can transfer partial light energy to heat. Carbon is a typical photothermal material, consequently, TL is much higher than TC indicating that it can convert more light energy into heat. In the case of Al_2O_3, TL is almost equal to TC, suggesting it has poor photothermal conversion capability. Overall, TL follows the order of C > Pd/C > Pd > Pd/Al_2O_3 > Al_2O_3. That implies that the carbon support has the highest photothermal conversion efficiency among all the species due to carbon being a photothermal material. Based on the above results, we proposed the following photo-assisted thermal mechanism (Fig. 5h). In the Pd/C system, carbon support can generate more heat than Pd nanoparticles under light irradiation, leading to the heat transfer from carbon to Pd nanoparticles. That makes the TL of Pd nanoparticles further increase and reach thermal equilibrium. The heat produced from carbon support is much larger than that from Pd nanoparticles, consequently, TL is decided by the carbon support. The presence of carbon support could be considered as a micro heating furnace, which enables in-situ heating of the active sites (Pd) through the photothermal effect. That agrees with Fig. 2d result which TC_{100} difference between dark and light remains almost the same at different loading Pd nanoparticles on the carbon support. On the other side, Al_2O_3 generates less heat than Pd nanoparticles in Pd/Al_2O_3. The heat will transfer from the Pd nanoparticle to the Al_2O_3 support. That is the reason why TL and TC of Pd/C are higher than those of Pd and lower than those of C. TL and TC of Pd/Al_2O_3 are lower than those of Pd and higher than those of Al_2O_3.

To demonstrate the excellent photothermal performance of carbon materials, we chose activated carbon (AC) loaded Pd catalysts for photothermal catalytic CO oxidation. As shown in Fig. S13a, the 1% Pd/AC catalyst exhibits typical diffraction peaks of carbon, but it is hard to observe Pd diffraction peaks. The Pd loading amount is too low to detect. TEM imaging disclose that the Pd NPs uniformly dispersed on AC (Fig. S13b). The nitrogen adsorption-desorption isotherms of AC showed typical microporous and mesoporous structures (Fig. S13c), and the surface area, pore-volume, and average pore size were 618.6 m^2/g, 0.72 cm^3/g, and 4.67 nm respectively. Meanwhile, the AC also exhibited excellent light absorption capability even after loading Pd nanoparticles (Fig. S14a). Next, the catalytic activities of 1% Pd/AC catalysts for CO oxidation are both evaluated under dark conditions and light irradiation with the intensity of 600 mW·cm^{-2}. In the dark condition, the lowest total conversion furnace temperature (TF_{100}) is 169 °C (Fig. S14b). Upon light irradiation, the catalyst temperature of 1% Pd/AC catalyst is rapidly risen to 71 °C within 5 min and finally maintain at 85 °C after 30 min without external heat (Fig. S14c). Furthermore, the catalytic performance over 1% Pd/AC catalyst is enhanced significantly when TF_{100} is 93 °C (Fig. S14b). And the contribution of different wavelengths of light radiation was carried out as well. The TF_{100} is 127 °C, 135 °C, and 139 °C under the illumination of IR, UV-Vis, and Vis, respectively. The percentage contribution of each fraction of light on the activity is 55.3%, 44.7%, and 39.1% for IR, UV–vis, and Vis (Fig. S14d), respectively. The above results further confirm the carbon-based material possessed excellent photothermal ability, which could convert solar light to thermal energy, to achieve the in-situ heating of active site Pd.

3.4. Photothermal catalytic stability and H_2O, CO_2, and SO_2 tolerance

The catalytic stability of the catalyst is a critical factor in industrial application. Hence, the on-stream test for the CO oxidation over Pd/C catalyst was carried out under the irradiation of 600 mW·cm^{-2}. As shown in Fig. 6a, CO conversion is stable at around 24% and 100%, respectively, during 24 h continuous testing. The used Pd/C catalyst after the reaction was characterized by XRD, TEM, and XPS as shown in Fig. S15, the crystal phase structure, particle size, and valence state barely changed, indicating the Pd/C catalyst possessed good catalytic stability.

The impurities, such as H_2O and SO_2 extensively exist in industrial exhaust emissions and automobile emissions, generally have a negative effort on the performance of catalysts. Therefore, the influences of H_2O and SO_2 on the photothermal catalytic activity for Pd/C catalyst are investigated. When 5 vol% and 10 vol% H_2O were introduced into the reaction system, the CO conversion has a gentle decrease (Fig. 6b), due

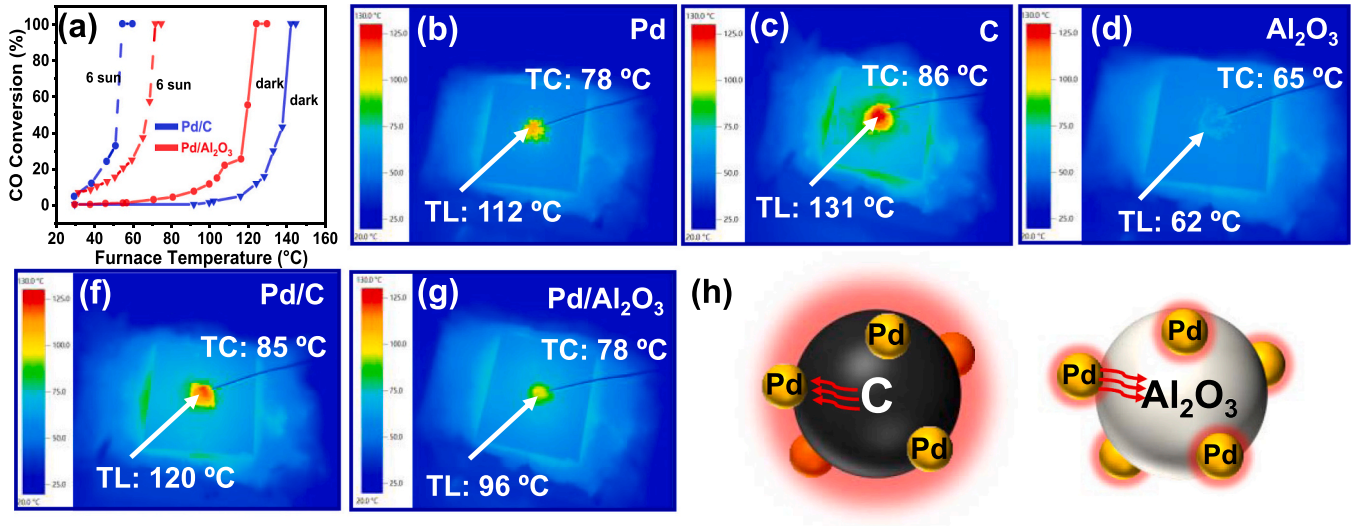

Fig. 5. (a) CO conversion over Pd/C and Pd/Al_2O_3 catalysts under the irradiation of 600 mW·cm^{-2}; (b–g) IR image over Pd, XC-72R, Al_2O_3, Pd/C, and Pd/Al_2O_3 samples with light irradiation of 200 mW·cm^{-2}; (h) Heat transfer mechanism over Pd/C and Pd/Al_2O_3 catalysts.

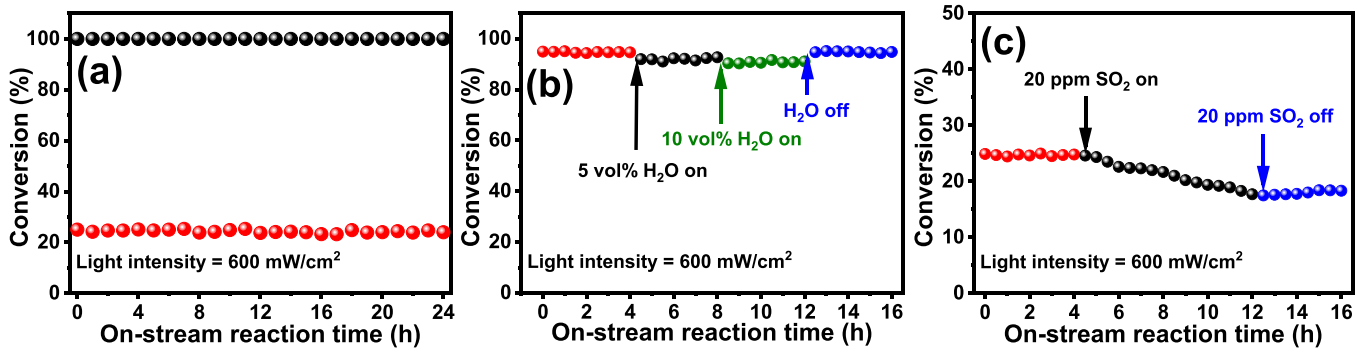

Fig. 6. (a) Catalytic stability, and effect of (b) H_2O and (c) SO_2 on the catalytic activity over 1% Pd/C for CO oxidation under light irradiation.

to the competitive absorption of CO, O_2, and H_2O on the active sites of Pd [36]. With the cut-off of water vapor, the conversion was recovered, indicating the deactivation led by water vapor was reversible. Differing from the absence of H_2O, the CO conversion gradually decreased from 25.0% to 17.5% with the introduction of 20 ppm SO_2. After cutting off SO_2, CO conversion had a little improvement but was far below initial CO conversion without SO_2 (Fig. 6c). This negative effect might be due to the accumulative adsorption of the SO_2 or form the sulfite species on the surface of Pd species [37].

4. Conclusion

In this work, a simple PVA-protected reduction method is adopted to prepare a Pd/C catalyst for a light-driven CO oxidation reaction. The introduction of light dramatically enhances the catalytic activity of CO oxidation, and the catalytic performance could be gradually enhanced with the increase of light intensity. Pd/C could realize the complete transformation at ambient temperature under the irradiation of 900 mW·cm^{-2}. However, Pd/C catalysts with different Pd loading have a similar performance enhancement under the same light irradiation, indicating Pd loading was not the major contributor to photothermal catalytic activity enhancement. Mechanism study demonstrated that Pd/C possessed a much higher local temperature than catalyst temperature under light irradiation and IR wavelength plays a major effort in elevating the catalyst temperature. Due to its excellent light-thermal conversion ability, carbon support holds a higher local temperature than Pd, so it could be regarded as a microheater to achieve in-situ heating of Pd. In summary, this study develops a promising purification technique for CO elimination and utilization of renewable solar energy.

CRediT authorship contribution statement

Ziwen Liu: Conceptualization, Methodology, Validation, Formal analysis, Investigation, Data curation, Writing – original draft. **Lijuan Niu:** Formal analysis, Investigation, Data curation. **Xupeng Zong:** Investigation. **Li An:** Investigation. **Dan Qu:** Investigation, Funding acquisition. **Xiayan Wang:** Writing – review & editing. **Zaicheng Sun:** Supervision, Conceptualization, Resources, Validation, Project administration, Funding acquisition.

Declaration of Competing Interest

There is no conflict-of-interest.

Acknowledgements

This study was financially supported by the Beijing Municipal High-Level Innovative Team Building Program (grant no. IDHT20180504), the Beijing Outstanding Young Scientists Program (BJJWZYJH01201910005017), the National Natural Science Foundation of China (grant nos. 21872001, 51801006, and 21805004), the Key Project of the National Natural Science Foundation of China (21936001 and 21801092), the Beijing Natural Science Foundation (grant no. 2192005), and the Beijing Municipal Science and Natural Science Fund Project (grant no. KM201910005016).

Appendix A. Supporting information

Supplementary data associated with this article can be found in the online version at doi:10.1016/j.apcatb.2022.121439.

References

[1] Y. Zhou, Z. Wang, C. Liu, Perspective on CO oxidation over Pd-based catalysts, Catal. Sci. Technol. 5 (2015) 69–81.
[2] P. Sudarsanam, B. Mallesham, P.S. Reddy, D. Großmann, W. Grünert, B.M. Reddy, Nano-Au/CeO_2 catalysts for CO oxidation: Influence of dopants (Fe, La and Zr) on the physicochemical properties and catalytic activity, Appl. Catal. B Environ. 144 (2014) 900–908.
[3] F. Morfin, T. Nguyen, J. Rousset, L. Piccolo, Synergy between hydrogen and ceria in Pt-catalyzed CO oxidation: An investigation on Pt–CeO_2 catalysts synthesized by solution combustion, Appl. Catal. B Environ. 197 (2016) 2–13.
[4] M.V. Grabchenko, G.V. Mamontov, V.I. Zaikovskii, V. La Parola, L.F. Liotta, O. V. Vodyankina, The role of metal–support interaction in Ag/CeO_2 catalysts for CO and soot oxidation, Appl. Catal. B Environ. 260 (2020), 118148.
[5] A. Satsuma, K. Osaki, M. Yanagihara, J. Ohyama, K. Shimizu, Activity controlling factors for low-temperature oxidation of CO over supported Pd catalysts, Appl. Catal. B Environ. 132–133 (2013) 511–518.
[6] G. Spezzati, A.D. Benavidez, A.T. DeLaRiva, Y. Su, J.P. Hofmann, S. Asahina, E. J. Olivier, J.H. Neethling, J.T. Miller, A.K. Datye, E.J.M. Hensen, CO oxidation by Pd supported on CeO_2(100) and CeO_2(111) facets, Appl. Catal. B Environ. 243 (2019) 36–46.
[7] B. Qiao, A. Wang, X. Yang, L.F. Allard, Z. Jiang, Y. Cui, J. Liu, J. Li, T. Zhang, Single-atom catalysis of CO oxidation using Pt_1/FeO_x, Nat. Chem. 3 (2011) 634–641.
[8] P. Schlexer, D. Widmann, R.J. Behm, G. Pacchioni, CO oxidation on a Au/TiO_2 nanoparticle catalyst via the Au-assisted Mars–van Krevelen mechanism, ACS Catal. 8 (2018) 6513–6525.
[9] L. Li, N. Zhang, X. Huang, Y. Liu, Y. Li, G. Zhang, L. Song, H. He, Hydrothermal stability of core–shell Pd@$Ce_{0.5}Zr_{0.5}O_2$/Al_2O_3 catalyst for automobile three-way reaction, ACS Catal. 8 (2018) 3222–3231.
[10] L. Li, N. Zhang, R. Wu, L. Song, G. Zhang, H. He, Comparative study of moisture-treated Pd@CeO_2/Al_2O_3 and Pd/CeO_2/Al_2O_3 catalysts for automobile exhaust emission reactions: effect of core–shell interface, ACS Appl. Mater. Interfaces 12 (2020) 10350–10358.
[11] W. Gao, B. Tian, W. Zhang, X. Zhang, Y. Wu, G. Lu, NIR light driven catalytic hydrogen generation over semiconductor photocatalyst coupling up-conversion component, Appl. Catal. B Environ. 257 (2019), 117908.
[12] T. Li, H. Liu, X. Zhao, G. Chen, J. Dai, G. Pastel, C. Jia, C. Chen, E. Hitz, D. Siddhartha, R. Yang, L. Hu, Scalable and highly efficient mesoporous wood-based solar steam generation device: localized heat, rapid water transport, Adv. Funct. Mater. 28 (2018) 1707134.
[13] M. Zhu, Y. Li, G. Chen, F. Jiang, Z. Yang, X. Luo, Y. Wang, S.D. Lacey, J. Dai, C. Wang, C. Jia, J. Wan, Y. Yao, A. Gong, B. Yang, Z. Yu, S. Das, L. Hu, Tree-inspired design for high-efficiency water extraction, Adv. Mater. 29 (2017) 1704107.
[14] Z. Lou, D. Yuan, F. Zhang, Y. Wang, Y. Li, L. Zhu, Fe_3Si assisted Co_3O_4 nanorods: a case study of photothermal catalytic CO oxidation under ambient solar irradiation, Nano Energy 62 (2019) 653–659.

[15] C. Dong, X. Zong, Z. Liu, L. Niu, Z. Zhao, L. An, D. Qu, X. Wang, Z. Sun, Light-promoted activation of oxygen and carbon monoxide for low-temperature catalytic oxidation, Cell Rep. Phys. Sci. 2 (2021), 100678.
[16] H. Liu, M. Li, T.D. Dao, Y. Liu, W. Zhou, L. Liu, X. Meng, T. Nagao, J. Ye, Design of PdAu alloy plasmonic nanoparticles for improved catalytic performance in CO_2 reduction with visible light irradiation, Nano Energy 26 (2016) 398–404.
[17] X. Meng, T. Wang, L. Liu, S. Ouyang, P. Li, H. Hu, T. Kako, H. Iwai, A. Tanaka, J. Ye, Photothermal conversion of CO_2 into CH_4 with H_2 over GroupVIII nanocatalysts: an alternative approach for solar fuel production, Angew. Chem. Int. Ed. 53 (2014) 11478–11482.
[18] Y. Zhai, Y. Dou, D. Zhao, P.F. Fulvio, R.T. Mayes, S. Dai, Carbon materials for chemical capacitive energy storage, Adv. Mater. 23 (2011) 4828–4850.
[19] H. Ren, M. Tang, B. Guan, K. Wang, J. Yang, F. Wang, M. Wang, J. Shan, Z. Chen, D. Wei, H. Peng, Z. Liu, Hierarchical graphene foam for efficient omnidirectional solar–thermal energy conversion, Adv. Mater. 29 (2017) 1702590.
[20] H. Ghasemi, G. Ni, A.M. Marconnet, J. Loomis, S. Yerci, N. Miljkovic, G. Chen, Solar steam generation by heat localization, Nat. Commun. 5 (2014) 4449.
[21] J. Wang, G. Zhang, P. Zhang, Graphene-assisted photothermal effect on promoting catalytic activity of layered MnO_2 for gaseous formaldehyde oxidation, Appl. Catal. B Environ. 239 (2018) 77–85.
[22] Y. Li, Y. Yu, J. Wang, J. Song, Q. Li, M. Dong, C. Liu, CO oxidation over graphene supported palladium catalyst, Appl. Catal. B Environ. 125 (2012) 189–196.
[23] L. Zhang, H. Liu, X. Huang, X. Sun, Z. Jiang, R. Schlögl, D. Su, Stabilization of palladium nanoparticles on nanodiamond–graphene core–shell supports for CO oxidation, Angew. Chem., Int. Ed. 54 (2015) 15823–15826.
[24] B. Qi, L. Di, W. Xu, X. Zhang, Dry plasma reduction to prepare a high performance Pd/C catalyst at atmospheric pressure for CO oxidation, J. Mater. Chem. A 2 (2014) 11885–11890.
[25] M. Comotti, W. Li, B. Spliethoff, F. Schüth, Support effect in high activity gold catalysts for CO oxidation, J. Am. Chem. Soc. 128 (2006) 917–924.
[26] I. Friberg, N. Sadokhina, L. Olsson, Complete methane oxidation over Ba modified Pd/Al_2O_3: the effect of water vapor, Appl. Catal. B Environ. 231 (2018) 242–250.
[27] D. Gao, C. Zhang, S. Wang, Z. Yuan, S. Wang, Catalytic activity of Pd/Al_2O_3 toward the combustion of methane, Catal. Commun. 9 (2008) 2583–2587.
[28] B. Lesiak, M. Mazurkiewicz, A. Malolepszy, L. Stobinski, B. Mierzwa, A. Mikolajczuk-Zychora, K. Juchniewicz, A. Borodzinski, J. Zemek, P. Jiricek, Effect of the Pd/MWCNTs anode catalysts preparation methods on their morphology and activity in a direct formic acid fuel cell, Appl. Surf. Sci. 387 (2016) 929–937.
[29] Y. Zhu, M. Chen, Y. Zhang, W. Zhao, C. Wang, A biomass-derived nitrogen-doped porous carbon for high-energy supercapacitor, Carbon 140 (2018) 404–412.
[30] B. Liu, M. Yang, H. Chen, Y. Liu, D. Yang, H. Li, Graphene-like porous carbon nanosheets derived from Salvia splendens for high-rate performance supercapacitors, J. Power Sources 397 (2018) 1–10.
[31] B. Chen, L.A. Crosby, C. George, R.M. Kennedy, N.M. Schweitzer, J. Wen, R.P. Van Duyne, P.C. Stair, K.R. Poeppelmeier, L.D. Marks, M.J. Bedzyk, Morphology and CO oxidation activity of Pd nanoparticles on $SrTiO_3$ nanopolyhedra, ACS Catal. 8 (2018) 4751–4760.
[32] P.G. O'Brien, A. Sandhel, T.E. Wood, A.A. Jelle, L.B. Hoch, D.D. Perovic, C. A. Mims, G.A. Ozin, Photomethanation of gaseous CO_2 over Ru/silicon nanowire catalysts with visible and near-infrared photons, Adv. Sci. 1 (2014) 1400001.
[33] X. Guo, C. Hao, C. Wang, S. Sarina, X. Guo, X. Guo, Visible light-driven photocatalytic Heck reaction over carbon nanocoil supported Pd nanoparticles, Catal. Sci. Technol. 6 (2016) 7738–7743.
[34] S. De Marchi, S. Núñez-Sánchez, G. Bodelón, J. Pérez-Juste, I. Pastoriza-Santos, Pd nanoparticles as a plasmonic material: synthesis, optical properties and applications, Nanoscale 12 (2020) 23424–23443.
[35] J. Jia, H. Wang, Z. Lu, P.G. O'Brien, M. Ghoussoub, P. Duchesne, Z. Zheng, P. Li, Q. Qiao, L. Wang, A. Gu, A.A. Jelle, Y. Dong, Q. Wang, K.K. Ghuman, T. Wood, C. Qian, Y. Shao, C. Qiu, M. Ye, Y. Zhu, Z. Lu, P. Zhang, A.S. Helmy, C.V. Singh, N. P. Kherani, D.D. Perovic, G.A. Ozin, Photothermal catalyst engineering: hydrogenation of gaseous CO_2 with high activity and tailored selectivity, Adv. Sci. 4 (2017) 1700252.
[36] F. Bi, X. Zhang, J. Chen, Y. Yang, Y. Wang, Excellent catalytic activity and water resistance of UiO-66-supported highly dispersed Pd nanoparticles for toluene catalytic oxidation, Appl. Catal. B Environ. 269 (2020), 118767.
[37] M.S. Wilburn, W.S. Epling, Formation and decomposition of sulfite and sulfate species on Pt/Pd catalysts: an SO_2 oxidation and sulfur exposure study, ACS Catal. 9 (2019) 640–648.